Mathematical modeling reveals alternative JAK inhibitor treatment in myeloproliferative neoplasms

Kaitlyn Shank,[1,2] Andrew Dunbar,[1] Priya Koppikar,[1] Maria Kleppe,[1] Julie Teruya-Feldstein,[3] Isabelle Csete,[1] Neha Bhagwat,[1,4] Matthew Keller,[1] Outi Kilpivaara,[1] Franziska Michor,[5,6,7] Ross L. Levine[1,4,8] and Laura de Vargas Roditi[9]

[1]Human Oncology and Pathogenesis Program, Memorial Sloan-Kettering Cancer Center, New York, NY, USA; [2]Penn State College of Medicine, Hershey, Pennsylvania, USA; [3]Department of Pathology, Icahn School of Medicine, Mount Sinai, New York, NY, USA; [4]Gerstner Sloan-Kettering Graduate School in Biomedical Sciences, Memorial Sloan-Kettering Cancer Center, New York, NY, USA; [5]Department of Biostatistics and Computational Biology, Center for Cancer Evolution, Dana-Farber Cancer Institute, Boston, MA, USA; [6]Department of Biostatistics, Harvard T.H. Chan School of Public Health, Boston, MA, USA, and Department of Stem Cell and Regenerative Biology, Harvard University, Cambridge, MA, USA; [7]The Broad Institute of Harvard and MIT, Cambridge, MA, USA and The Ludwig Center at Harvard, Boston, MA, USA; [8]Leukemia Service, Memorial Sloan-Kettering Cancer Center, NY, USA and [9]Institute of Molecular Cancer Research, University of Zurich, Zurich Switzerland

Correspondence: LAURA DE VARGAS RODITI. - laura.devargasroditi@uzh.ch

doi:10.3324/haematol.2018.203729

SUPPLEMENTAL MATERIALS AND METHODS

Ruxolitinib (INCB018424)
Ruxolitinib (INCB018424) is a potent and selective JAK1/2 inhibitor that was approved in 2011 for the treatment of myelofibrosis and polycythemia vera(1). The approval was based on the drug's ability to significantly reduce splenomegaly and ameliorate symptoms through the suppression of JAK2V617-mediated signaling(2). The ruxolitinib used in this study was synthesized by Incyte and stored at room temperature. A stock solution of the drug was prepared every seven days in citrate buffer with 20% captisol. The vehicle was composed of citrate buffer with 20% captisol. For *in vitro* experiments, ruxolitinib was prepared in DMSO in 1 mM concentrations and stored at -20 degrees Celsius, and underwent no more than three freeze-thaw cycles.

Murine model, in vivo dosing schedule and analysis of mice
A conditional *Jak*2V617F knock-in model of polycythemia vera(3) in a CD45.2 background was used for this murine study. Bone marrow from this model was extracted and transplanted into lethally irradiated CD45.1 background recipient mice (see Bone Marrow Transplantation section). Fourteen days post-transplantation, blood counts were collected and mice were randomized into four groups: vehicle, 60 mg/kg ruxolitinib BID, 270 mg/kg ruxolitinib BID five days on and two days off, and 360 mg/kg ruxolitinib BID three days on and four days off. There were five mice in each group.

The average weight for all mice was 0.02 kg and no significant weight loss was observed throughout the study. For the vehicle group, 200 uL vehicle was administered BID for the duration of the study. For the 60 mg/kg group, a stock solution of 60 mg/mL ruxolitinib was prepared and 200 uL were administered to the mice BID. For the 270 mg/mL group, a stock solution of 180 mg/mL ruxolitinib was prepared and 300 uL were administered to the mice BID for five days, followed by a two-day holiday. For the 360 mg/kg group, two doses of 200 uL of 180 mg/mL were administered approximately ten minutes apart BID for three days, followed by a four day holiday (Figure S4). The daily BID treatments were administered approximately 8 hours apart.

All mice were treated with oral gavage for 25 days or until one of the criteria for sacrificing them was met following the guidelines of Memorial Sloan-Kettering Cancer Center Institutional Animal Care and Use Committee- approved animal protocol. Differential blood counts were assessed by submandibular bleeds at two weeks and at the conclusion of the study. Peripheral blood, liver, spleen, bone marrow, and gut were collected at the conclusion of the study. For histopathology, tissues were fixed in 4% paraformaldehyde and then formalin-fixed paraffin-embedded tissue sections were stained using hematoxylin and eosin. Tissue sections were evaluated by a hematopathologist. Bone marrow, spleen and liver cells were collected for flow cytometry.

Bone marrow transplantation
Dissected femurs and tibias from the conditional *Jak*2V617F knock-in model of polycythemia vera(3). in a CD45.2 background were isolated. Bone marrow was spun at 8,000 rpm in a PCR tube (with a perforated tip) within an Eppendorf tube for 1 min into 10% fetal calf serum (FCS) media to flush bones. Cells were passed through a 70 uM strainer. Red blood cells (RBCs) were lysed in ammonium chloride-potassium bicarbonate lysis buffer for 10 min on ice. Cells were then mixed 3:2 with CD45.1 C57BL/6 marrow and 2 million cells were tail vein injected into 20 lethally irradiated CD45.1 C57BL/6 recipients (Figure S4).

Flow cytometry
For the *in vitro* studies, cells were washed in cold phosphate buffered saline (PBS), spun, and then washed in 1X Annexin Binding Buffer. The cells were then spun and resuspended in 1X Annexin Binding Buffer at $5x10^6$/mL. FITC-conjugated Annexin V stain and 7AAD stain were added to 100uL of cell suspension and incubated at room temperature for 15 minutes, protected from light. Data were collected on BD Biosciences LSRFortessa without washing and analysis was performed on FlowJo.

For the *in vivo* studies, bone marrow and spleen cells were filtered, and red blood cells were lysed and washed in 1X PBS. For chimerism staining, cells were incubated with the following antibodies for 30 minutes on ice in PBS plus 2% bovine serum albumin (BSA): CD11b conjugated to fluorescein isothiocyanate (FITC) (BioLegend), CD45.1 conjugated to eFluor 450 (eBioscience), and CD45.2 conjugated to APC (BioLegend). Data were collected on BD Biosciences LSRFortessa and analysis was performed on FlowJo.

Western Blot

Splenocytes were collected from all experimental and control arms at the time of either their death or the conclusion of the study (25 days), whichever came first, after dosing with the assigned ruxolitinib or control regimen. The mice were sacrificed 2 hours after their final drug treatment, after which cells were extracted, processed and frozen down for Western Blot analysis at a later date. To process the splenocytes, they were passed through a 70 uM filter. Red blood cells were lysed in ammonium chloride-potassium bicarbonate lysis buffer for 10 min on ice. Cells were then spun down and snap frozen on dry ice. Upon thawing at a later date, cells were resuspended in lysis buffer (150 mM NaCl, 20 mM Tris [pH 7.4-7.5], 5 mM ethylenediaminetetraacetic acid, 1% Triton-X, 10% glycerol) containing Protease Arrest (G-Biosciences), Phosphatase Inhibitor Cocktail II (EMD Chemicals). Protein was quantified using the Bio-Rad Bradford protein estimation and 30 to 50 ug was loaded per well in 4% to 12% Bis-Tris electrophoresis gels (Invitrogen). Protein was transferred on to 0.45-micron nitrocellulose membranes. Antibodies used for western blotting included pSTAT3, STAT3, pSTAT5, STAT5 (all from Cell Signaling Technologies) and beta actin.

Cell lines

SET-2 cells (megakaryoblastic cell line established from the peripheral blood of a patient with leukemic transformation of essential thrombocythemia (ET)) were cultured in RPMI-1640 supplemented with 20% FBS.

In vitro assays for determining birth and death rates

SET-2 cells were cultured with varying concentrations of ruxolitinib ranging through 0, 0.1, 0.5, 1 and 2 μM. For each drug concentration, approximately 6 million cells were diluted in 12mL of media in tissue culture flasks and cultured for 48 hours. Three replicate 500uL samples of cell culture were counted at 0, 24 and 48 hours (for each drug concentration) with cell viability analyzer, Vi-cell (Beckman-Coulter), to estimate the total population size at a given time point. Also for each time point and drug concentration, a 1mL sample from each culture was stained with an apoptosis and a viability marker (FITC-Annexin V and 7AAD, respectively; BD Pharmingen) and 50,000 events were analyzed with flow cytometry using a FACScalibur in order to distinguish what portion of the total population consisted of live, dead, and apoptotic cells (Figure 1A, S1). The data obtained through flow cytometry was analyzed using FlowJo software (Tree Star Inc). Determining these proportions through flow cytometry was crucial to assess the birth and death rates of the cells treated with varying drug concentrations (Figure 1B, S2). However, we must point out that measurements can fluctuate depending on the viability and variability (given different passages) of the cells at the beginning of the experiment since each experimental replicate was not done at the same starting point but rather months apart. Also, the sampling taken from the population at each time point can introduce further variability in the estimated cell counts. Since ultimately a cell line is only an approximation of the *in vivo* reality, we take into consideration all the variability encountered from the *in vitro* experiments into our modelling. To fairly assess the trend given by all three replicates taken altogether, we estimate the fit for 100 separate bootstrapping samples re-sampled from all points from all replicates. More details about how the birth and death rates are estimated will be described in detail in the mathematical model section.

Pharmacokinetic analysis

An exponentially decaying surface (Figure 1E) was used to model drug plasma concentration over time for multiple doses (pharmacokinetic analysis done by Incyte, data not shown). A negative exponential surface was chosen by combining the simplest canonical

pharmacokinetic model of an exponential decay of plasma concentration as a function of dose and the linear relationship between dose and plasma concentration. The surface has the following functional form: $plasma(dose, time) = \alpha * dose * e^{-\beta * time}$. The model parameters were estimated using a non-linear least absolute residuals regression.

The mathematical model

To enable re-use of our materials and improve reproducibility and transparency we include the MATLAB code and data used for all the analysis and visualizations contained in this paper in the open repository https://github.com/answermyriddles/rux.

The *in vitro* flow cytometric data allowed us to estimate the population of live, apoptotic and dead cells and these estimates were used to calculate birth and death rates (Figure S2). The change in live cells after a certain time interval, ΔL, corresponds to the number of cells that were born (ΔB) minus the number cells that died (ΔD) in that interval of time: $\Delta L = \Delta B - \Delta D$. Therefore, the rate of change in birth is defined by the rate of change in live cells plus the rate of change in dead cells: $\frac{\Delta B}{\Delta t} = \frac{\Delta L}{\Delta t} + \frac{\Delta D}{\Delta t}$. We denote $b = \frac{\Delta B}{\Delta t}$ and $d = \frac{\Delta D}{\Delta t}$. The death rate was then calculated as $\frac{\Delta D}{\Delta t} = \frac{\Delta D(b-d)}{\Delta L}$. For the purpose of the calculations described above, the population of apoptotic cells was incorporated into the population of dead cells. The cells' birth rates and death rates were fit to experimental data (Figures S1 and S2). The Bayesian Information Criterion was used to choose the best-fitting model (Figure S2). A linear model was chosen for the birth rate following:

$$birth(concentration) = \alpha_b + \beta_b * concentration$$

and a logarithmic model was chosen for the death rate following:

$$death(concentration) = \alpha_d * \ln(\gamma_d + \beta_d * concentration)$$

To determine the optimal dosing strategy that would minimize the number of cancer cells after treatment, we investigated how varying drug concentrations and treatment schedules differentially affected cell growth. We decided to describe cell proliferation over time as an exponential growth model where the parameters are the cell's birth and death rates (*b* and *d*, respectively), which are themselves functions of the drug concentration:

$p_{t_2} = p_{t_1} e^{(b-d)\Delta t}$,

where p_{t_2} and p_{t_1} denote the number of cells at time t_2 and t_1, respectively and $\Delta t = t_2 - t_1$ thus $t_2 > t_1$. We initialize the population size at the beginning of our simulation with 10^6 cells, approximating the number of cancer cells injected in our murine model.

The administration of different concentrations of drug affects the cells' birth and death rates differently; our mathematical model allows us to estimate the cell population size after a given combination of drug dose and treatment length, i.e. a dosing strategy, as in previous studies(4, 5). We divided the treatment into cycles of seven days and each cycle consisted of a pulse, T_{on} (an interval of time Δt when the drug was being administered) and a break, T_{off} (an interval of time Δt when the drug was not being administered) (Figure 1C). We can interpret a schedule where T_{off} is zero (there are no breaks) to the equivalent of a chronic dose treatment.

We fit our pharmacokinetic data with an exponentially decaying surface (Figure 1E), which allowed us to describe the expected plasma concentration of the drug over time. The pharmacokinetic analysis revealed that ruxolitinib plasma concentration decreased significantly, in between dose administrations. The twice daily dosing was done in intervals of 8 and 16 hours, and the pk data suggested that during the latter, cells were exposed to a much lower drug concentration long before the next dose was administered, which could

result in fluctuating cell growth rates in between doses. To account for this possibility, instead of assuming that cells grow at a constant growth rate during both intervals between doses, we updated the cell growth rate, eight hours later, given the expected ruxolitinib plasma concentration at that time point.

The *in vitro* data used to estimate the birth and death rates showed considerable variability. We hypothesize that there was either technical or biological variability and to study how this variability affected our conclusions we performed a robustness analysis. For the birth rate, we fit each of the replicates individually with a regression model and ran a statistical test (t-test) which revealed that the slopes of replicates 1 and 3 were in fact not significantly different from zero (p-value = 0.06018 and p-value = 0.0600). Replicate 2 suggested a negative slope significantly different from zero (p-value = 0.0378). This suggested different trends for replicates 1 and 3 (unchanged with drug concentration) and replicate 2 (decreasing with drug concentration). We therefore simulated the model considering a birth rate fit to each replicate separately with zero slopes for replicates 1 and 3 (Supplemental figure 7). Replicates 1 and 3 suggested that an intermittent treatment of 270mg/kg was more efficacious than a chronic treatment while replicate two suggested all intermittent treatments were more efficacious. However, as we were aware of the noise in the in vitro data and made a conservative choice to only test in vivo intermittent treatment doses of 270mg/kg and 360mg/kg.

Although the death rate estimates showed consistent trends across replicates, there were still considerable fluctuations, therefore we included an additional analysis for each birth rate but now for a range of death rate functions (Supplemental figure 8) to illustrate that the simulations for each birth rate were consistent for the whole range of death rate functions. All showed that birth rates fit to replicate 2 would suggest all intermittent dosing strategies to be more beneficial while birth rates fit to replicates 1 and 3 would suggest an intermittent treatment of 270mg/kg, regardless of the choice of death function in the range of our death rate data.

Toxicity constraint

Following the *in vitro* studies where we determined the birth and death rates of SET-2 cells in the presence of different concentrations of ruxolitinib (Figure S2), our aim was to find the combination of dose and treatment length that would minimize the number of JAK2V617F cells after a four-week treatment period. Thus, we were interested in the dose that resulted in the lowest birth rate and highest death rate of the cancer cells. The death rate of cells is a monotonically increasing function of the drug dose, which would imply that the best dosing strategy would be an infinitely high dose administered indefinitely. However, this is an unrealistic treatment, as it does not take into account the toxicity resulting from high doses of the drug. This is especially true as ruxolitinib is a JAK2 inhibitor and wildtype JAK2 is essential for promoting normal cell growth. In order to determine the optimal dosing schedule, we constrained the model to a range of treatment schedules tolerated in mice. This toxicity constraint was built using previously derived preclinical data (Incyte personal communication), which indicated the maximum number of days a particular dose was tolerated (Figure S3) including that the maximum tolerated chronic dose was 60 mg/kg given daily and that 600 mg/kg could only be safely administered for a maximum of 1 day (longer treatment resulted in death). Unfortunately, the data available was very limited, containing only three data points, which only allowed for a very rough estimate of the toxicity constraint (Figure S3), and could only be fit with a simple linear model. However, as expected, the data supports that the number of days tolerated as a function of dose is monotonically decreasing; that is, the lower the dose, the longer it can be safely administered.

Acknowledgements

We would like to thank Jasmine Foo and members of the Michor and Levine laboratories for the many fruitful discussions that guided this research. We also thank Dorothea Ruthishauser and Ana Filipa Gonçalves for feedback on the manuscript. We thank the Mullally laboratory for providing us with the breeder Jak2V617F mouse for our colony.

Author contribution

In regards to author contribution, K.S., F.M., R.L.L. and L.D.V.R. conceived the study. K.S. and L.D.V.R. performed all experiments with help from A.D., P.K., N.B., M.K., I.C., and O.K.. L.D.V.R and K.S. performed the *in vitro* experiments with help from O.K. while K.S. performed the *in vivo* experiments with help from A.D., P.K. N.B., M.K. and I.C.. The analysis of pathology slides was performed by J.T.. L.D.V.R. developed the mathematical model and performed computational simulations. K.S., F.M., R.L.L. and L.D.V.R wrote the manuscript. All authors provided feedback on the manuscript.

Disclosures

R.L.L. is on the supervisory board of Qiagen and is a scientific advisor to Loxo, Imago, C4 Therapeutics and Isoplexis, which each include an equity interest. He receives research support from and consulted for Celgene and Roche, he has received research support from Prelude Therapeutics, and he has consulted for Incyte, Novartis, Morphosys and Janssen. He has received honoraria from Lilly and Amgen for invited lectures and from Gilead for grant reviews.

This work was supported by NCI P01 CA108671 and NCI R35197594 to R.L.L, by the Janus Project to R.L.L, and by a LLS SCOR grant to R.L.L. Studies supported by MSK core facilities were supported in part by MSKCC Support Grant/Core Grant P30 CA008748.

References

1. Harrison C, Kiladjian JJ, Al-Ali HK, Gisslinger H, Waltzman R, Stalbovskaya V, et al. JAK inhibition with ruxolitinib versus best available therapy for myelofibrosis. N Engl J Med. 2012;366(9):787-98.
2. Bhagwat N, Koppikar P, Keller M, Marubayashi S, Shank K, Rampal R, et al. Improved targeting of JAK2 leads to increased therapeutic efficacy in myeloproliferative neoplasms. Blood. 2014;123(13):2075-83.
3. Mullally A, Lane SW, Ball B, Megerdichian C, Okabe R, Al-Shahrour F, et al. Physiological Jak2V617F expression causes a lethal myeloproliferative neoplasm with differential effects on hematopoietic stem and progenitor cells. Cancer Cell. 2010;17(6):584-96.
4. Foo J, Michor F. Evolution of resistance to targeted anti-cancer therapies during continuous and pulsed administration strategies. PLoS Comput Biol. 2009;5(11):e1000557.
5. Chmielecki J, Foo J, Oxnard GR, Hutchinson K, Ohashi K, Somwar R, et al. Optimization of dosing for EGFR-mutant non-small cell lung cancer with evolutionary cancer modeling. Sci Transl Med. 2011;3(90):90ra59.

Figure S1. Flow cytometric analysis of SET-2 cells treated with ruxolitinib. SET-2 cells were treated with a range of Ruxolitinib (0, 0.1, 0.5, 1 and 2 uL) for 48 hours. Samples were taken every 24 hours and stained with 7-AAD and FITC-Annexin V for determining live, dead, and apoptotic cell populations.

Figure S2. Birth, death and overall growth rates. Birth and death rates determined based on flow cytometric analysis of SET-2 cells in the presence of Ruxolitinib at different concentrations. The x-axis shows the drug concentrations to which cells were exposed and the y-axis shows (A) the birth and (B) death rates resulting from different concentrations of drug exposure. Mean lines correspond to a model fit to all the data and shaded region shows the 95% confidence interval obtained from 100 bootstrapping samples. (C) Bayesian information criteria was used to compare different possible models and a linear model was chosen for having the lowest BIC. (D) Bayesian information criteria was also used to inform the death rates however, although a linear model had the lowest BIC it resulted in very high death rates and fast death of the cells in the population growth simulation, so we opted for the second best model (logarithmic) which had more biologically plausible predictions. It is important to point out that both the linear and the log model suggested the same two intermittent treatments for testing and therefore choosing one or the other would not have informed the *in vivo* experiments differently.

Figure S3. Toxicity constraint. Consecutive days mice have been shown to tolerate various doses of Ruxolitinib before the dose becomes toxic (evaluated by death).

Figure S4. *In vivo* studies of intermittent vs. chronic ruxolitinib dosing. CD45.2-Jak2V617F BM was harvested and mixed with CD45.1-C57BL/6 BM at a 3:2 ratio before injection into lethally irradiated CD45.1-C57BL/6 recipients. After two weeks, these recipients were randomized based on complete blood counts and divided into four experimental groups of 5 mice each. The first group was treated via gavage with vehicle BID for 7 days a week. The second group was treated via gavage with 60 mg/kg ruxolitinib BID for 7 days a week. The third group was treated via gavage with 270 mg/kg ruxolitinib BID for 5 days a week. Finally, the fourth group was treated via gavage with 360 mg/kg for 3 days a week. CBCs were evaluated at the beginning of each week and the trial concluded after 25 days, when the organs were harvested for analysis.

Figure S5. Red blood cell (RBC), white blood cell (WBC) and platelet (PLT) counts measured before treatment, 2-weeks into treatment and at the conclusion of the study for vehicle, chronic 60 mg/kg ruxolitinib and intermittent 270 mg/kg ruxolitinib arms. Data shows some reduction in RBC (significant with $p<0.016$) and WBC (non-significant with $p>0.1$) counts in the 270 mg/kg group compared to 60 mg/kg but no noticeable change across groups in PLT counts (see Table 1 for all pairwise Wilcoxon rank sum test comparisons).

Figure S6. H & E staining of bone marrow, liver, spleen and gut of *Jak2*V617F mice treated with vehicle or ruxolitinib throughout the course of the trial. i) **Bone Marrow**: A) Vehicle, relative erythroid hyperplasia. B) 60mpk, trilineage hematopoiesis with increased numbers of megakaryocytes. C) 270 mpk, unremarkable trilineage hematopoiesis. D) 360 mpk, unremarkable trilineage hematopoiesis. ii) **Liver:** A) Vehicle, portal and lobular inflammation present B) 60 mpk, unremarkable with no overt pathologic change. C) 270 mpk, minimal to absent portal and lobular inflammation. D) 360 mpk, absent portal and lobular inflammation. iii) **Spleen:** A) Vehicle, unremarkable spleen B) 60 mpk, unremarkable spleen (C) 270 mpk, white, red pulp preserved, focal extramedullary hematopoiesis. D) 360 mpk, White pulp preserved, focal extramedullary hematopoiesis. iv) **Gut:** A) Vehicle, unremarkable intestinal mucosa. B) 60 mpk, mild focal chronic inflammation C) 270 mpk. unremarkable intestinal mucosa D) 360 mpk, unremarkable intestinal mucosa.

Table S1. Wilcoxon rank sum test p-value results on pairwise comparisons between treatment groups show non-significant changes in liver weight between vehicle and both 60mpk and 270mpk treatment groups and indicate no increased liver toxicity in the 270mpk treated cohort. Spleen weight comparisons show a significant difference between the larger spleens from the vehicle group versus the smaller spleens in both 60mpk and 270mpk groups, however no significant difference between spleen sizes in the two treatment groups (60mpk vs 270mpk). Differences between the 270mpk group and two others were significant for hemoglobin and hematocrit, supporting the improved efficacy of the 270mpk treatment at reducing these blood parameters. Differences in white blood cells (WBC) and platelets (PLT) values were non-significant in all pairwise groups comparisons.

Figure S7. Robustness analysis. A. Birth rates fit to each individual replicate from in vitro experiments. B-D Treatment schedules simulated for each birth rate function fit to each replicate.

Figure S8. Robustness analysis for a range of Death rates. A. Death rate functions estimated from fitting all data (Fit All) as described in the methods while varying the logarithmic parameter (b in log(bx)) such that the range of functions provide coverage of the data range. B-D Treatment schedules simulated for birth rate functions fit to each replicate for death rate function sens1 ($b_{sens1} = 1.5*b_{all}$). E-G Treatment schedules simulated for birth rate functions fit to each replicate for death rate function sens2 (($b_{sens1} = 2*b_{all}$)).H-J Treatment schedules simulated for birth rate functions fit to each replicate for death rate function sens3

($b_{sens1} = 0.7*b_{all}$). K-M Treatment schedules simulated for birth rate functions fit to each replicate for death rate function sens4 ($b_{sens1} = 0.4*b_{all}$).

Figure S1.

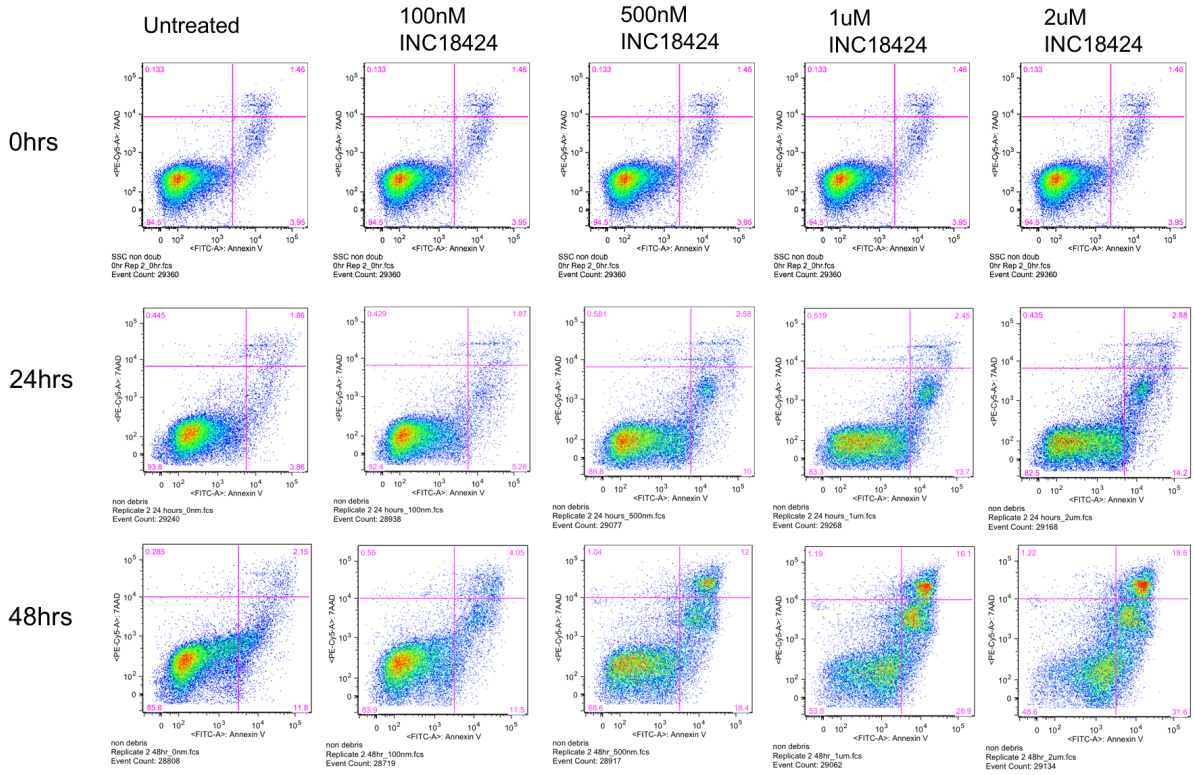

Figure S2.

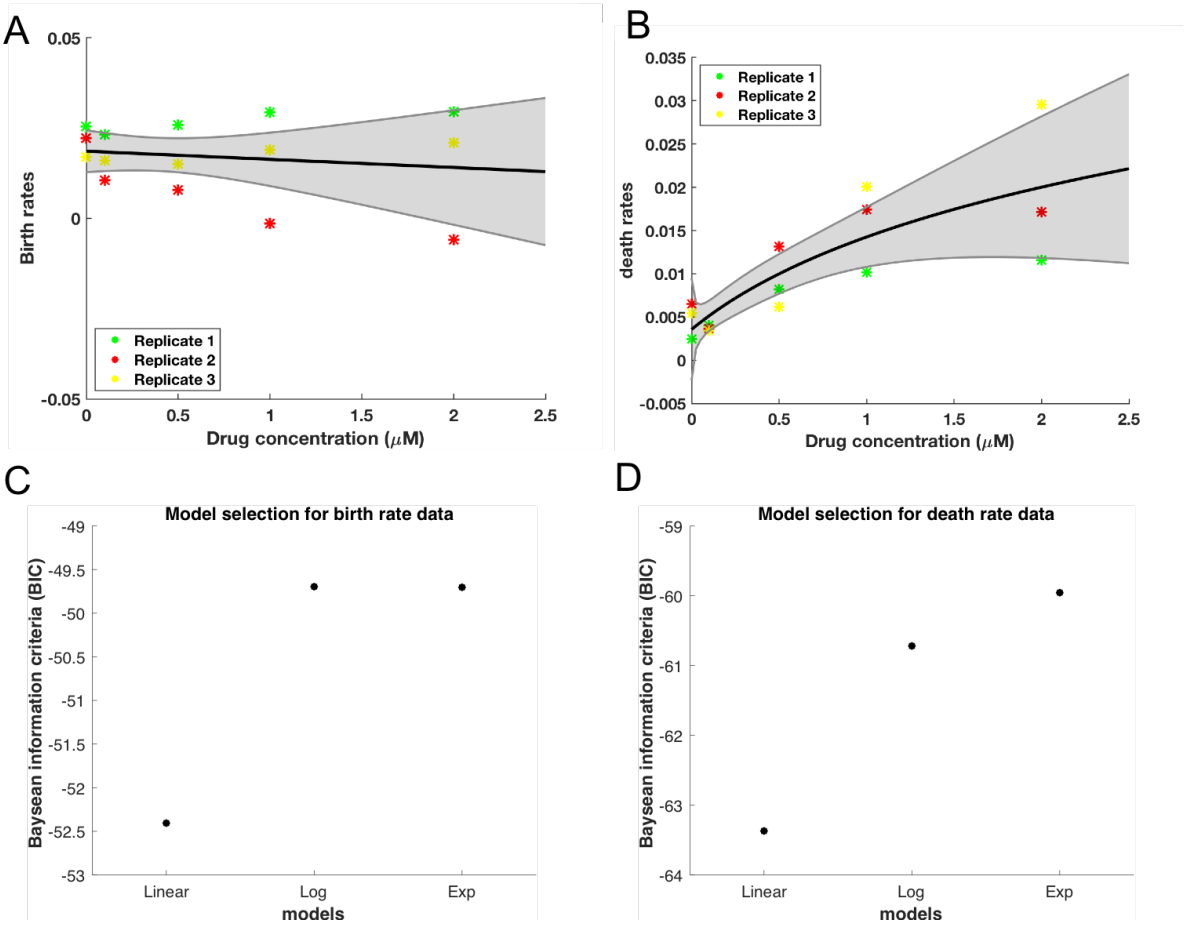
A
Birth rates
Drug concentration (μM)
Replicate 1
Replicate 2
Replicate 3
B
death rates
Drug concentration (μM)
Replicate 1
Replicate 2
Replicate 3
C
Model selection for birth rate data
Baysean information criteria (BIC)
Linear
Log
Exp
models
D
Model selection for death rate data
Baysean information criteria (BIC)
Linear
Log
Exp
models

Figure S3.

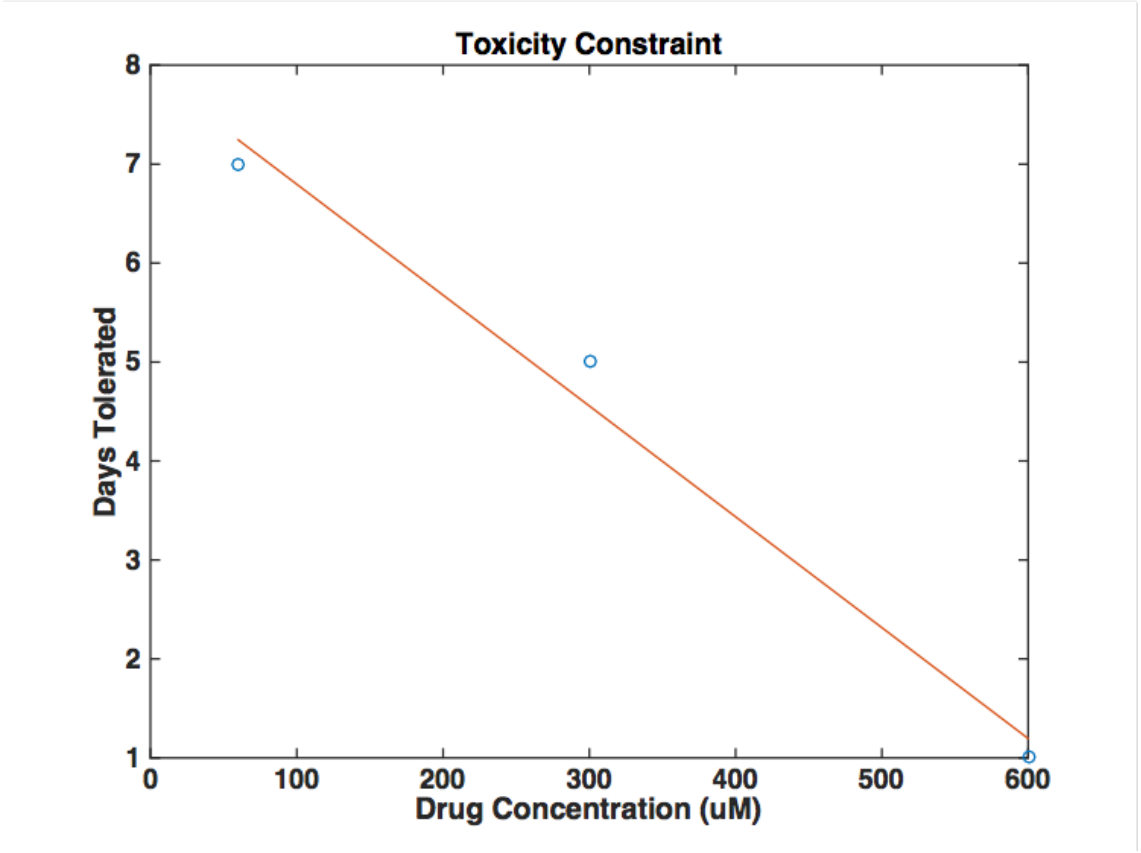

Figure S4.

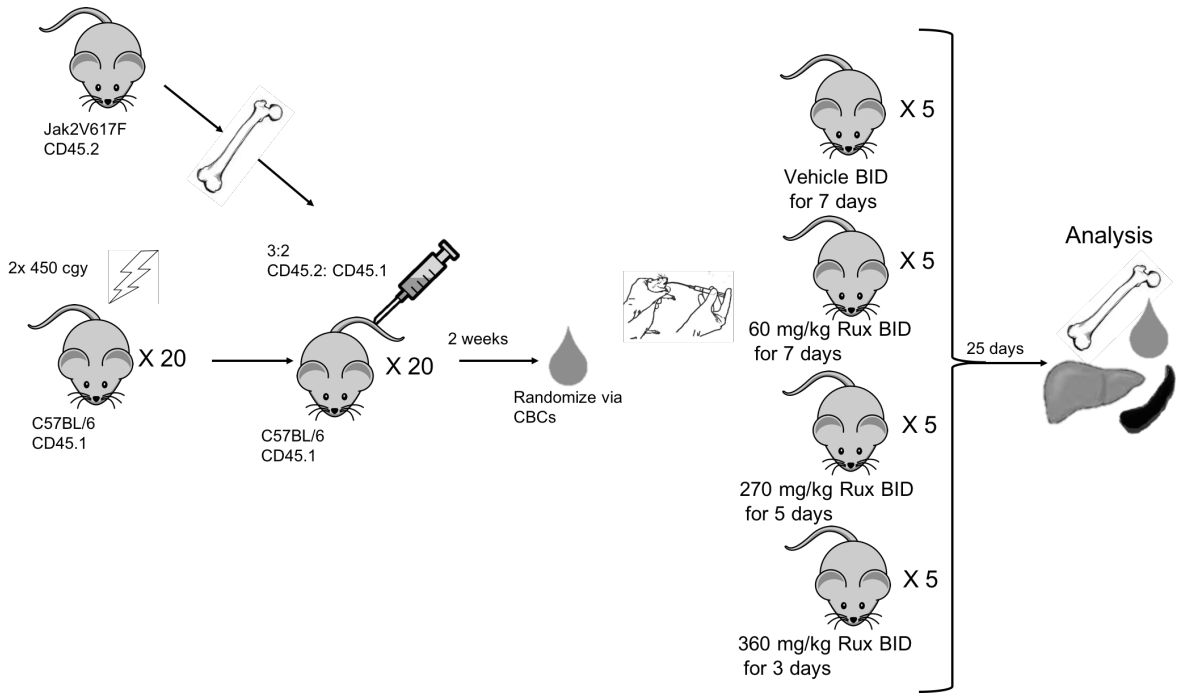

Figure S5.

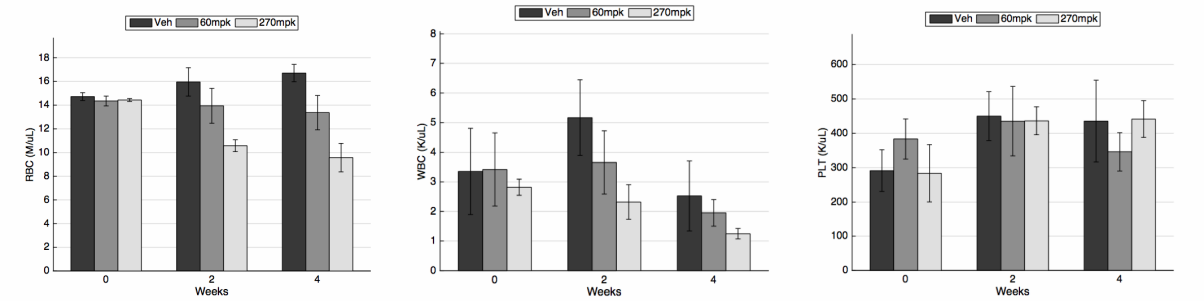

Figure S6.

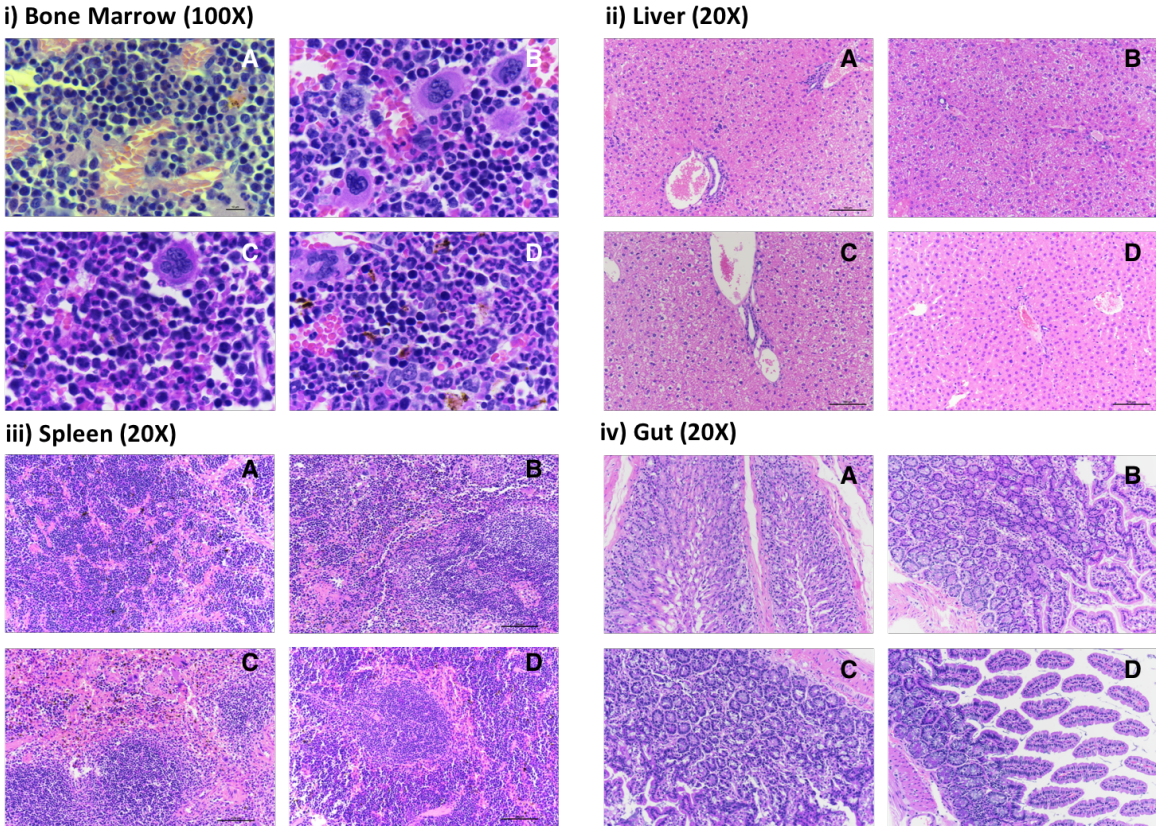

Table S1.

Group1	Groups2	WBC	PLT	HCT	HGB	RBC	Liver	Spleen
Veh	60mpk	0.420634921	0.222222222	0.222222222	0.46031746	0.007936508	1	0.007936508
Veh	270mpk	0.031746032	0.904761905	0.015873016	0.015873016	0.015873016	0.150793651	0.007936508
60mpk	270mpk	0.111111111	0.063492063	0.015873016	0.015873016	0.015873016	0.150793651	1

Figure S7.

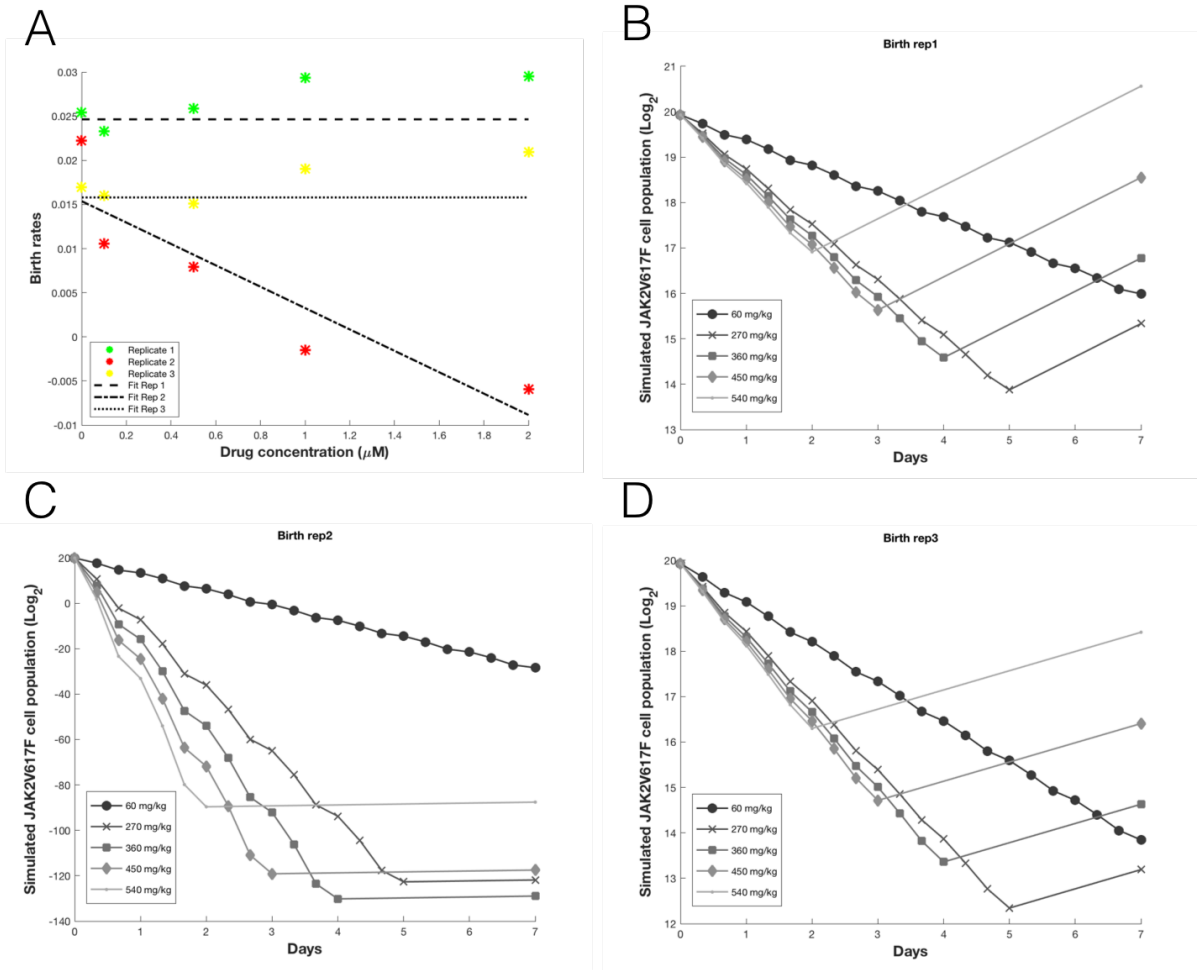
A
Birth rates
Drug concentration (μM)
Replicate 1
Replicate 2
Replicate 3
Fit Rep 1
Fit Rep 2
Fit Rep 3
B
Birth rep1
Simulated JAK2V617F cell population (Log2)
Days
60 mg/kg
270 mg/kg
360 mg/kg
450 mg/kg
540 mg/kg
C
Birth rep2
Simulated JAK2V617F cell population (Log2)
Days
60 mg/kg
270 mg/kg
360 mg/kg
450 mg/kg
540 mg/kg
D
Birth rep3
Simulated JAK2V617F cell population (Log2)
Days
60 mg/kg
270 mg/kg
360 mg/kg
450 mg/kg
540 mg/kg

Figure S8.

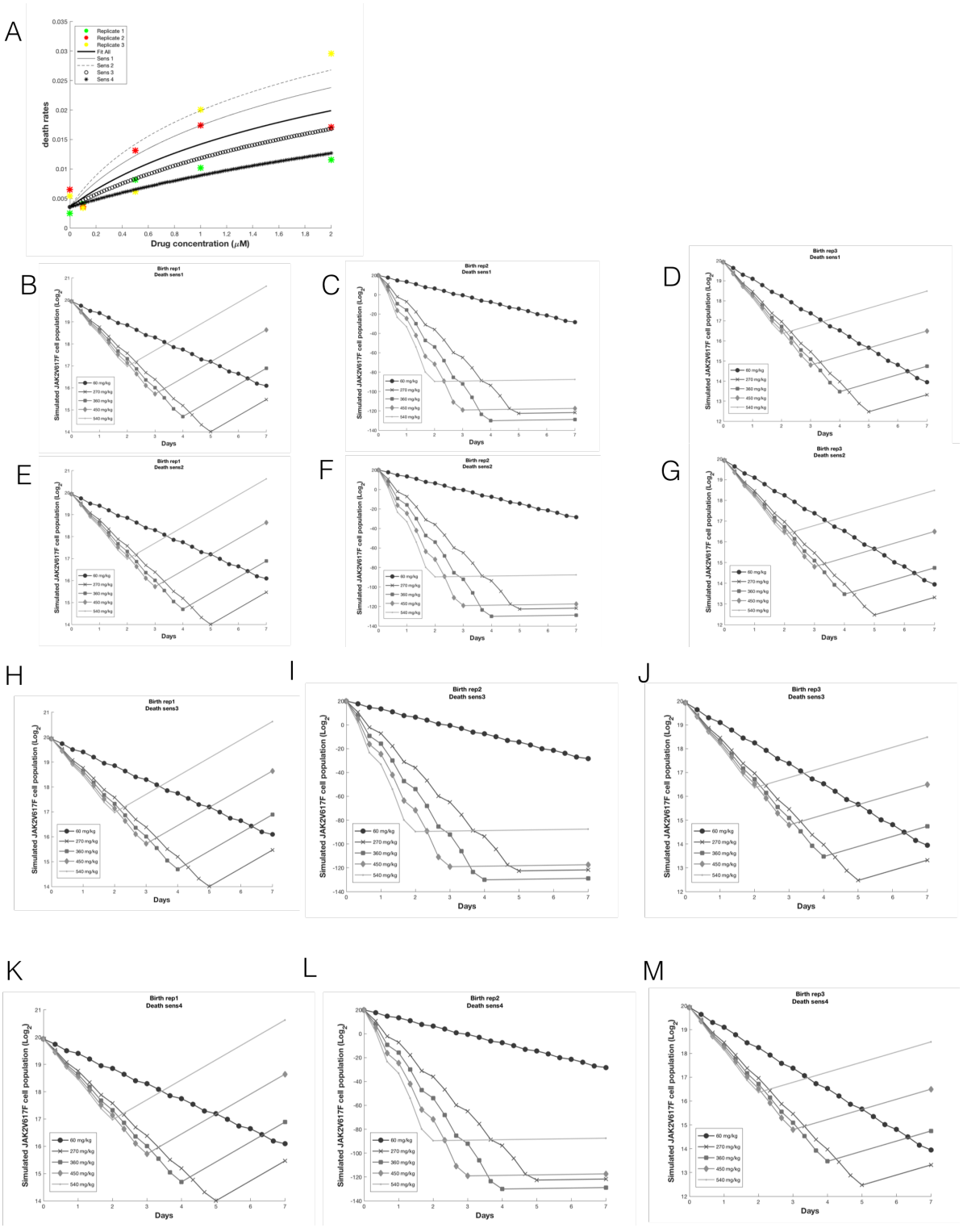
A
Replicate 1
Replicate 2
Replicate 3
Fit All
Sens 1
Sens 2
Sens 3
Sens 4
death rates
Drug concentration (μM)
B
Birth rep1
Death sens1
C
Birth rep2
Death sens1
D
Birth rep3
Death sens1
E
Birth rep1
Death sens2
F
Birth rep2
Death sens2
G
Birth rep3
Death sens2
H
Birth rep1
Death sens3
I
Birth rep2
Death sens3
J
Birth rep3
Death sens3
K
Birth rep1
Death sens4
L
Birth rep2
Death sens4
M
Birth rep3
Death sens4
Simulated JAK2V617F cell population (Log2)
Days
60 mg/kg
270 mg/kg
360 mg/kg
450 mg/kg
540 mg/kg